

S-DCCRN: SUPER WIDE BAND DCCRN WITH LEARNABLE COMPLEX FEATURE FOR SPEECH ENHANCEMENT

Shubo Lv¹, Yihui Fu¹, Mengtao Xing¹, Jiayao Sun¹, Lei Xie¹, Jun Huang², Yannan Wang², Tao Yu²

Audio, Speech and Language Processing Group (ASLP@NPU),
Northwestern Polytechnical University, Xi'an, China
Tencent Ethereal Audio Lab, Tencent Corporation, Shenzhen, China

ABSTRACT

In speech enhancement, complex neural network has shown promising performance due to their effectiveness in processing complex-valued spectrum. Most of the recent speech enhancement approaches mainly focus on wide-band signal with a sampling rate of 16K Hz. However, research on super wide band (e.g., 32K Hz) or even full-band (48K) denoising is still lacked due to the difficulty of modeling more frequency bands and particularly high frequency components. In this paper, we extend our previous deep complex convolution recurrent neural network (DCCRN) substantially to a super wide band version – S-DCCRN, to perform speech denoising on speech of 32K Hz sampling rate. We first employ a cascaded sub-band and full-band processing module, which consists of two small-footprint DCCRNs – one operates on sub-band signal and one operates on full-band signal, aiming at benefiting from both local and global frequency information. Moreover, instead of simply adopting the STFT feature as input, we use a complex feature encoder trained in an end-to-end manner to refine the information of different frequency bands. We also use a complex feature decoder to revert the feature to time-frequency domain. Finally, a learnable spectrum compression method is adopted to adjust the energy of different frequency bands, which is beneficial for neural network learning. The proposed model, S-DCCRN, has surpassed PercepNet as well as several competitive models and achieves state-of-the-art performance in terms of speech quality and intelligibility. Ablation studies also demonstrate the effectiveness of different contributions.

Index Terms— speech enhancement, super wide band, S-DCCRN

1. INTRODUCTION

With the fast development of tele-conference and other real-time speech communication scenarios, the demand for high-quality Hi-Fi speech has increased sharply. With a higher sampling rate, speech will contain richer information and more fine details, especially in higher frequency bands. However, most current deep learning based speech enhancement approaches mainly focus on wide band signal at sampling rate of 16K Hz. The potential of speech enhancement on super wide band [1] or even full-band signal is still to be explored since the challenges exist in modeling more frequency bands and particularly high frequency components. Moreover, modeling with larger dimensional features will cause higher complexity of the modeling, making real-time implementation becomes more difficult. Some speech enhancers have adopted compressed features like bark spectrum [2] to model high frequency signal while feature compression may unavoidably lose important information of frequency bands, resulting in sub-optimal performance.

For a long time, DNN-based speech front-end algorithms attempt to only enhance the noisy magnitude while the noisy phase

is directly incorporated for speech waveform reconstruction. The reasons can be attributed to the unclear structure of the phase, which is considered challenging to estimate. Subsequently, complex ratio mask (CRM) [3] was proposed by Williamson *et al.*, which can reconstruct speech perfectly by enhancing both real and imaginary components of the noisy speech simultaneously. Wide-band scenario based SOTA methods like SDD-Net [4] and DCCRN [5] have shown outstanding performance, especially for complex denoising cases with low SNRs and sudden noise. DCCRN combines the advantages of both DCUNET [6] and CRN [7], using LSTM to model temporal context with significantly reduced trainable parameters and computational cost. SDD-Net applies the power-compressed spectrum [8] as the input features and employs four particularly designed stages, which dramatically improved speech quality in simultaneous dereverberation and denoising. For full-band scenario, studies in RNNoise [2] adopt bark spectrum, instead of STFT, as the input of the model. Bark spectrum only has 22 dimensions on frequency axis totally [9], which can reduce the model size to a great extent and speed up model inference. The bark spectrum assumes that the spectral envelopes of the speech and noise are flat sufficiently [2]. However, this method may lead to severe attenuation in the real acoustic scenario due to the complexity of the real acoustic scenario (such as sudden noises and reverberation), which leads to excessive noise residual. Very recently, the PercepNet [10] proposed a perceptual band representation which operates on only 32 triangular spectral bands, spaced according to the equivalent rectangular bandwidth (ERB) scale [9]. However, the resolution of bark scale and ERB scale are more rough than linear spectrum from STFT, leading to the leakage of information of frequency bands. Speech enhancement on super wide band/full-band signal has drawn much attention recently – deep noise suppression challenge (DNS) [11] has particularly set up a full-band track.

This paper proposes *super wide band* DCCRN (S-DCCRN) for speech enhancement in super wide-band scenarios at 32K Hz sampling rate. The contribution of this work is three-fold, evaluated objectively on Voicebank and Demond dataset and subjectively on DNS-2021 blind test set.

We propose two lightweight DCCRN sub-modules for *sub-band* and *full-band* (SAF) modeling respectively, since it is considered that low frequency bands contain higher energy while higher frequency bands have a great impact on subjective perception [12]. Therefore, sub-band processing module is employed to model low frequency bands and high frequency bands separately. However, only adopting sub-band processing may cause unsmooth connection among frequency bands since there is no explicit information interaction between low- and high-frequency components. Thus, we further apply a full-band processing module to smooth the bound-

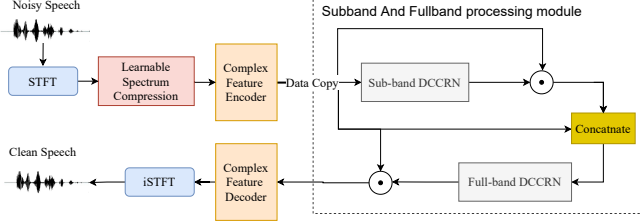


Fig. 1. Network structure of the proposed *S*-DCCRN

aries of different frequency bands. In detail, the sub-band processing module consists of a sub-band DCCRN, which substitute the complex convolution of original DCCRN with group complex convolution to model low-frequency bands and high-frequency bands separately. The convolution pathways [13] among encoder and decoder of both full-band and sub-band processing modules are used for better information interaction avoiding information lost in full-band. With a smaller model size, the SAF module leads to 0.17 PESQ improvement compared with the oracle DCCRN.

Inspired by spectrum compression in wide-band denoising [8], we introduce *learnable spectrum compression* (LSC) in our model, which can dynamically adjust the energy of different frequency bands. The use of LSC results in more clear patterns on the high-frequency bands and this update brings an extra PESQ gain of 0.07.

Motivated by the encoder/decoder block of the DPT-FSNet [14], we employ a *complex feature encoder* (CFE) after STFT and a *complex feature decoder* (CFD) before iSTFT. We keep the same STFT points as most wide-band speech enhancement models. Although the frequency resolution is relatively low for high sampling rate scenario, the CFE block can refine the information of different frequency bands of the STFT spectrum. With learnable spectrum compression, this update brings an extra PESQ gain of 0.07.

The proposed *S*-DCCRN model surpasses all tested SOTA models, including RNNNoise and DCCRN, and obtains superior performance with 3.62 MOS score on the blind test set of Interspeech 2021 DNS challenge [11].

2. SUPER WIDE BAND DCCRN (S-DCCRN)

2.1. Complex Feature Encoder/Decoder

Researchers usually adopt Bark spectrum as the input of the network for full-band speech enhancement in wide band scenario, which can convert physical frequency to psychoacoustic frequency based on human perception [2]. However, the original physical frequency bands are compressed through this conversion, and the phase information is discarded as well. In addition, features based on the human perception may not be suitable for the input of network. On the other hand, using the STFT features directly also causes certain problems. With a larger number of points of STFT, the network complexity will increase due to high-dimensional input features that are hard to model. On the contrary, the use of the STFT features with a smaller number of points can also cause the degradation of frequency resolution. In this paper, inspired by the encoder/decoder block of DPT-FSNet [14], we adopt a complex feature encoder/decoder after STFT to refine the information of different frequency bands based on 512-dimensional complex STFT features.

As shown in Figure 2 (a), the input of the complex feature encoder (CFE) module is the T-F spectrum obtained by STFT. We employ complex conv2d with a kernel size of 1 to extract high-dimensional information. Then a dilated dense block [15] is used to capture long-term contextual features from time scale. Finally, a complex conv2d is adopted to extract complex local features. Layer-Norm and PReLU activation are successively performed after each convolution.

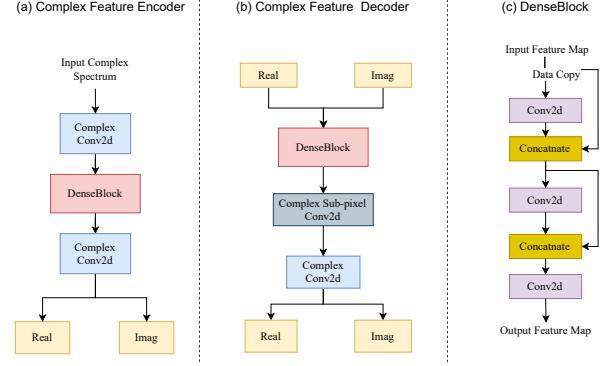


Fig. 2. Complex feature encoder/decoder (CFE/CFD) module

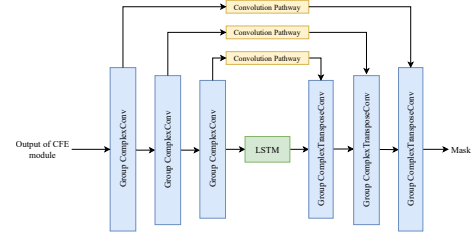


Fig. 3. The sub-band DCCRN module

As shown in Figure 2 (b), the input of the complex feature decoder (CFD) module is the real/imag features of the output of SAF module. In detail, we employ the dilated dense block to process the estimated real/imag features. Then the output of dilated dense block is processed by complex pixel convolution, which substitute the convolution in the pixel convolution [16] with complex convolution. The pixel convolution is considered as a better alternative for transposed convolution to avoid checkerboard artifacts [17]. Finally, a complex convolution is performed to revert the high-dimensional feature to the time-frequency domain. As shown in Figure 2 (c), each dense block consists of five layers of conv2d. The convolutions across the frames are causal. The dense connection to all the previous layers avoids the vanishing gradient problem [15].

2.2. Sub-band and Full-band Processing Module

As the sampling rate increases, the number of frequency bands also increases to a great extent. Different frequency bands are hard to be modeled by only full-band processing because the information among low-frequency and high-frequency is substantially different [12]. It is not optimal to model them within one module. On the other hand, sub-band processing can cause a certain unsmooth connection at the boundary of different frequency bands since there is no information interaction among different bands. Based on the considerations mentioned above, we propose a sub-band And full-band processing (SAF) module to take the advantage from both.

As shown in Figure 1, we use the encoded feature from CFE as the input of the SAF module, which is mainly composed of a sub-band DCCRN and a full-band DCCRN. In the SAF module, the features are firstly processed by a sub-band DCCRN. The concatenation of the sub-band DCCRN output together with the encoded feature from CFE, which is considered to help to smooth frequency bands, is treated as the input of the full-band DCCRN. The output of full-band DCCRN is the complex ratio mask (CRM) of the encoded feature from CFE.

The structure of the sub-band DCCRN is shown in Figure 3. The general design of the sub-band DCCRN is similar to the oracle DCCRN, but the complex convolution block in oracle DCCRN

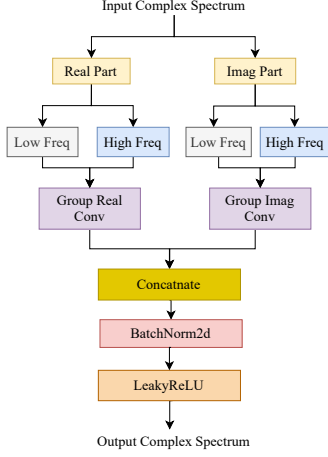


Fig. 4. Complex group convolution

is substituted with a complex group convolution block. As shown in Figure 4, complex group convolution block aims to model low-frequency bands and high-frequency bands separately. In addition, to aggregate richer information from each encoder layer and relieve the unsmooth connection among frequency bands, we employ the convolution pathway block between encoder and decoder, which was proven useful in DCCRN+ [13]. Specifically, the convolution pathway between encoder and decoder consists of a complex convolution block and batch normalization.

After concatenating the encoded feature from CFE together with the output of sub-band DCCRN, we use another full-band DCCRN, which takes ordinary complex convolution instead of complex group convolution, to further regenerate and smooth different frequency bands. Full-band DCCRN also employs the convolution pathway among encoder and decoder for better information interaction.

2.3. Learnable Spectrum Compression

It is pointed out that local patterns in the spectrum are often different in each frequency band: the lower frequency band tends to contain high energies, tonalities as well as long sustained sounds, while the higher frequency band is likely to have low energy components, noise, and rapidly decaying sounds [12]. Recently, spectrum compression on wide-band denoising has shown promising results, which can increase the energy of the high-frequency bands through a compression rate of 0.5 [8].

We believe that the compression rate of frequency bands should be different since high-frequency bands may require a lower compression ratio to maintain its high energy. This inspires us to develop a learnable spectrum compression module using a set of network layers to compress the STFT spectrum. The sigmoid activation is performed after the learnable network layers, aiming to compress the output to $0 \sim 1$. In detail, the learnable spectrum compression can be described as

$$Y_{LSC} = |Y|^\alpha e^{j\varphi_Y} \quad (1)$$

where Y and α denote the noisy spectrum and the learnable parameters respectively.

2.4. Loss Function

For the learning objective, we first apply SI-SNR [18] loss, which is a time-domain loss function. Furthermore, we employ complex mean-squared error (MSE) loss and the Kullback-Leibler Divergence [19] to improve the similarity between the estimated spectrum and the clean spectrum in complex domain. The purpose of KL Divergence is to optimize clean and estimated spectrum from the perspective of probability distribution. The three losses are optimized jointly by:

$$\begin{cases} \mathcal{L}_{\text{cMSE}} &= \frac{1}{T \times F} \sum_{t,f} \left| |X| e^{j\varphi_X} - |\hat{X}| e^{j\varphi_{\hat{X}}} \right| \\ \mathcal{L}_{\text{KL}} &= \frac{1}{T \times F} \sum_{t,f} \hat{X} \cdot \log\left(\frac{\hat{X}}{X}\right) \\ \mathcal{L} &= \mathcal{L}_{\text{SI-SNR}} + \mathcal{L}_{\text{cMSE}} + \mathcal{L}_{\text{KL}} \end{cases} \quad (2)$$

where \hat{X} and X denote the network output and clean spectrum respectively. We omit the dependency of the target speech spectral bins $X_{t,f}$ on the frequency and time indices t, f for brevity.

3. EXPERIMENTS

3.1. Datasets

We carry out speech enhancement experiments on audio samples with 32K sampling rate. We firstly conduct ablation experiments to prove the effectiveness of each proposed sub-modules on Voice Bank and DEMAND dataset [20]. Specifically, the source speech comes from the VoiceBank corpus [21], which contains 28 speakers for training and another 2 speakers for testing. Ten noise types with two artificially generated and eight real recordings from DEMAND [22] are used for training. Note that all data are downsampled from 48 K to 32K Hz before experimentation. Totally, the fixed training and validation set contains 11,572 utterances (10 h), and 872 utterances (30 min), respectively. We also compare other SOTA models (including PercepNet [10]) with S-DCCRN on this dataset.

Then S-DCCRN is further trained and evaluated with the Interspeech 2021 DNS challenge dataset to show its performance on more complicated and real acoustic scenarios. The source speech data comes from DNS-2021 full-band dataset, which contains 672 h speech data. The 180-hour DNS-2021 noise set, which includes 65,000 noise clips from 150 noise classes, is selected as the source noise data. The training set contains 605 h source speech data, while the validation set contains 67 h source speech data respectively. The training data are generated on-the-fly with 32K Hz sampling rate and segmented into 8 s chunks in one batch with SNR ranges from -5 to 20 dB. The total data ‘seen’ by the model is more than 9000 h after 14 epochs of training.

3.2. Training setup and baselines

For the proposed models, the window length and frame shift are 15ms and 5ms, respectively, resulting in a 20 ms at runtime of the model. The STFT length is 512. For the models trained on Voice Bank and DEMAND dataset, all models are trained for 36 epochs with the following learning rate schedule: a constraint learning rate of 0.000025 is used for the first 10 epochs to warmup; then the learning rate is reset to 0.001. For the models trained on DNS-2021 dataset, the initial learning rate is 0.001 and will get halved if there is no loss decrease on the validation set. We also compare the proposed S-DCCRN model and its ablation components on the Voice Bank and DEMAND dataset with other SOTA models. They are described as follows.

DCCRN: The number of channels for the DCCRN is {16,32,64,128,256,256}, and the convolution kernel and step size are set to (5,2) and (2,1) respectively. Two LSTM layers are adopted and the number of nodes is 256. There is a 1024×256 fully connected layer after the LSTM. Each encoder/decoder module handles the current frame and one previous frame.

S-DCCRN: The number of channels for the sub-band DCCRN is {32,64,64,64,128,128}, and the convolution kernel and step size are set to (5,2) and (2,1) respectively. In addition, the channel number of the first layer of full-DCCRN is 64. One LSTM layer is adopted by sub-band DCCRN and full-band DCCRN respectively and the number of nodes is 256. There is a 256×256 fully connected layer after the LSTM. Each encoder/decoder module handles the current frame and one previous frame. The hidden channels of the complex feature encoder/decoder module are 32, and the depth

of DenseBlock is 5. LayerNorm and PReLU are performed after each convolution, except for the last layer of the CFD module.

3.3. Experimental results and discussion

As presented in Table 1, ablation studies are conducted to evaluate the effectiveness of different model components of *S*-DCCRN, including a) sub-band processing module (SP), b) sub-band and full-band processing module (SAF), c) *S*-DCCRN without complex feature encoder/decoder module (CFE/CFD), d) *S*-DCCRN without CFE/CFD and substitute learnable spectrum compression (LSC) with spectrum compression (SC), e) substitute LSC with SC. It should be noted that the SP only consists of a sub-band DCCRN, and thus the number of channels of encoder and decoder are $\{2, 64, 64, 128, 128, 256\}$. The LSTM layers and units of SP are 2 and 256 respectively. We adopt CSIG, COVL, CBAK [23], STOI [24] and PESQ [25] as five evaluation metrics.

Table 1. Results of various models and ablation experiments on Voice Bank and DEMAND set.

Model	# Para.(M)	PESQ	CSIG	COVL	CBAK	STOI
Noisy	-	1.97	3.35	2.63	2.44	0.921
RNNNoise	0.06	2.34	3.40	2.84	2.51	0.922
PercepNet	8	2.73	-	-	-	-
DCCRN	3.7	2.54	3.74	3.13	2.75	0.938
SP	2.76	2.63	3.86	3.23	3.03	0.935
SAF	2.73	2.71	3.94	3.31	3.08	0.937
+ SC	2.73	2.76	3.98	3.36	2.87	0.938
+ LSC	2.73	2.77	3.98	3.35	2.92	0.938
+ CFE/CFD	2.34	2.69	3.90	3.28	3.08	0.939
+ SC	2.34	2.77	3.98	3.37	2.87	0.940
+ LSC (<i>S</i> -DCCRN)	2.34	2.84	4.03	3.43	2.97	0.940

It can be seen from the results that the performance of the SAF module is obviously better than DCCRN, which obtains 0.17 PESQ improvement with a smaller model size. Compared with SP module, SAF module yielded 0.08 PESQ improvement. Because the low frequency and high frequency are modeled separately in the information of different frequency bands cannot be integrated. Adding CFE/CFD block yields lower PESQ compared to the SAF module alone. The low PESQ performance is caused by the low energy of high frequency, which is difficult for CFE/CFD block to model. This problem can be solved by adding a spectrum compression block. In addition, the results indicate that the proposed learnable spectrum compression is more effective than traditional spectrum compression [8] and it is especially beneficial for CFE/CFD block. It is worth to note that our approach achieves 0.11 PESQ improvement compared to Percepnet.

In Figure 5, we show the learned compression ratio of different frequency bands on our denoising systems. We can observe that for the frequency bands lower than 13K Hz, the spectrum compression rate gradually decreases as the frequency increases. When frequency is higher than 13K Hz, the compression rate first increases and then

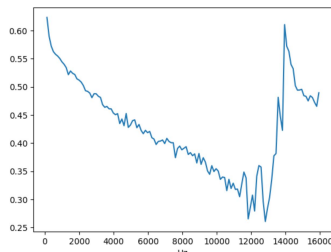


Fig. 5. Compression ratio of different frequency automatically learned by the proposed learnable spectrum compression.

stabilizes at about 0.5. We can consider that the low-frequency band has relatively larger energy and is unnecessary to be compressed to a great extent. In addition, the high-frequency bands demand a lower compression ratio to amplify the energy. Furthermore, the information of higher frequency bands is relatively few, which is not necessary to be deeply compressed. The spectrum after applying the traditional spectrum compression [8] and learnable spectrum compression are shown in Figure 6. With the help of the learnable approach, the components of low-frequency band is not suppressed too much due to the high compression rate. Additionally, the speech and noise in the high-frequency band are more clear, leading to better noise reduction.

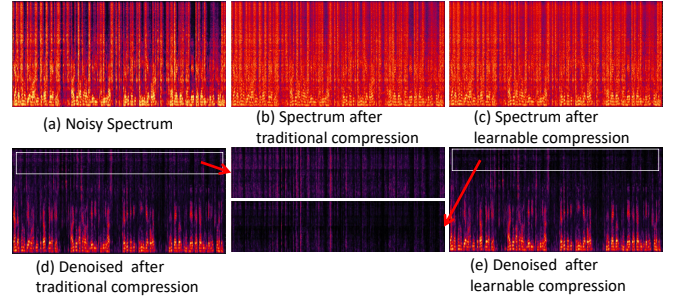


Fig. 6. Comparison on the denoising result on a testing noisy clip for the cases with/without learnable spectrum compression.

We further evaluate the models trained on the DNS-2021 dataset. Subjective tests are conducted by 10 listeners with aired hearing to evaluate the speech quality and intelligibility, in terms of 5-point mean opinion score (MOS) [26], i.e., 1-bad, 2-poor, 3-fair, 4-good, 5-excellent on randomly selected 20 utterances. We also downsample the enhanced waveform to 16K Hz and conduct a DNSMOS evaluation¹ [27], which is used to simulate the human subjective evaluation. As shown in Table 2, with more training data, the MOS and DNSMOS for the SAF module are restored to the same level as DCCRN. When CFE/CFD and LSC modules are applied, the *S*-DCCRN further improves the scores and achieves state-of-the-art performance.

Table 2. MOS and DNSMOS results on DNS-2021 blind test set.

Model	MOS	DNSMOS*
Noisy	1.66	2.94
RNNNoise	2.32	3.07
DCCRN	3.30	3.31
SAF	3.20	3.33
<i>S</i> -DCCRN	3.62	3.43

*: Calculated on downsampled speech (16K Hz)

4. CONCLUSIONS

In this paper, we propose a novel super wide-band STFT domain denoising network running on 32K signal. The *S*-DCCRN is equipped with SAF module via a cascaded sub-band and full-band processing module, aiming at benefiting from both local and global frequency information processing. Importantly, a complex feature encoder/decoder is adopted to refine the information of different frequency bands. Finally, a learnable spectrum compression method is employed to adjust the energy of different frequency bands. The proposed *S*-DCCRN model obtains superior performance with 3.62 MOS score on the blind test set of Interspeech 2021 DNS challenge. Experiments have shown the effectiveness of these methods².

¹DNSMOS only supports 16k Hz sampling rate

²Demo page is available at <https://imybo.github.io/S-DCCRN/>

5. REFERENCES

- [1] Richard V Cox, Simao Ferraz De Campos Neto, Claude Lamblin, and Mostafa Hashem Sherif, "Itu-t coders for wideband, superwideband, and fullband speech communication [series editorial]," *IEEE Communications Magazine*, vol. 47, no. 10, pp. 106–109, 2009.
- [2] Jean-Marc Valin, "A hybrid dsp/deep learning approach to real-time full-band speech enhancement," in *2018 IEEE 20th international workshop on multimedia signal processing (MMSP)*. IEEE, 2018, pp. 1–5.
- [3] Donald S Williamson, Yuxuan Wang, and DeLiang Wang, "Complex ratio masking for monaural speech separation," *IEEE/ACM transactions on audio, speech, and language processing*, vol. 24, no. 3, pp. 483–492, 2015.
- [4] Andong Li, Wenzhe Liu, Xiaoxue Luo, Guochen Yu, Chengshi Zheng, and Xiaodong Li, "A Simultaneous Denoising and Dereverberation Framework with Target Decoupling," *Interspeech*, pp. 2801–2805, 2021.
- [5] Yanxin Hu, Yun Liu, Shubo Lv, Mengtao Xing, Shimin Zhang, Yihui Fu, Jian Wu, Bihong Zhang, and Lei Xie, "DCCRN: Deep complex convolution recurrent network for phase-aware speech enhancement," *Interspeech*, pp. 2472–2476, 2020.
- [6] Hyeon-Seok Choi, Jang-Hyun Kim, Jaesung Huh, Adrian Kim, Jung-Woo Ha, and Kyogu Lee, "Phase-aware speech enhancement with deep complex u-net," in *International Conference on Learning Representations*, 2018.
- [7] Ke Tan and DeLiang Wang, "A convolutional recurrent neural network for real-time speech enhancement," in *Proc. Interspeech*, 2018, pp. 3229–3233.
- [8] Andong Li, Chengshi Zheng, Renhua Peng, and Xiaodong Li, "On the importance of power compression and phase estimation in monaural speech dereverberation," *JASA Express Letters*, vol. 1, no. 1, pp. 014802, 2021.
- [9] Brian CJ Moore, *An introduction to the psychology of hearing*, Brill, 2012.
- [10] Jean-Marc Valin, Umut Isik, Neerad Phansalkar, Ritwik Giri, Karim Helwani, and Arvinth Krishnaswamy, "A perceptually-motivated approach for low-complexity, real-time enhancement of fullband speech," *Interspeech*, pp. 2482–2486, 2020.
- [11] Chandan KA Reddy, Harishchandra Dubey, Kazuhito Koishida, Arun Nair, Vishak Gopal, Ross Cutler, Sebastian Braun, Hannes Gamper, Robert Aichner, and Sriram Srinivasan, "INTERSPEECH 2021 Deep Noise Suppression Challenge," *Interspeech*, pp. 2796–2800, 2021.
- [12] Naoya Takahashi and Yuki Mitsufuji, "Multi-scale multi-band densenets for audio source separation," in *Proc. ASPAA*. IEEE, 2017, pp. 21–25.
- [13] Shubo Lv, Yanxin Hu, Shimin Zhang, and Lei Xie, "DC-CRN+: Channel-Wise Subband DCCRN with SNR Estimation for Speech Enhancement," *Interspeech*, pp. 2816–2820, 2021.
- [14] Feng Dang, Hangting Chen, and Pengyuan Zhang, "DPT-FSNet: Dual-path Transformer Based Full-band and Sub-band Fusion Network for Speech Enhancement," *arXiv preprint arXiv:2104.13002*, 2021.
- [15] Ashutosh Pandey and DeLiang Wang, "Densely connected neural network with dilated convolutions for real-time speech enhancement in the time domain," in *ICASSP 2020-2020 IEEE International Conference on Acoustics, Speech and Signal Processing (ICASSP)*. IEEE, 2020, pp. 6629–6633.
- [16] Wenzhe Shi, Jose Caballero, Ferenc Huszár, Johannes Totz, Andrew P Aitken, Rob Bishop, Daniel Rueckert, and Zehan Wang, "Real-time single image and video super-resolution using an efficient sub-pixel convolutional neural network," in *Proceedings of the IEEE conference on computer vision and pattern recognition*, 2016, pp. 1874–1883.
- [17] Augustus Odena, Vincent Dumoulin, and Chris Olah, "Deconvolution and checkerboard artifacts," *Distill*, vol. 1, no. 10, pp. e3, 2016.
- [18] Yi Luo and Nima Mesgarani, "Conv-tasnet: Surpassing ideal time-frequency magnitude masking for speech separation," *IEEE/ACM transactions on audio, speech, and language processing*, vol. 27, no. 8, pp. 1256–1266, 2019.
- [19] Daniel Polani, "Kullback-leibler divergence," *Encyclopedia of Systems Biology*, pp. 1087–1088, 2013.
- [20] Cassia Valentini-Botinhao, Xin Wang, Shinji Takaki, and Junichi Yamagishi, "Investigating RNN-based speech enhancement methods for noise-robust Text-to-Speech," in *Proc. SSW*, 2016, pp. 146–152.
- [21] Christophe Veaux, Junichi Yamagishi, and Simon King, "The voice bank corpus: Design, collection and data analysis of a large regional accent speech database," in *2013 international conference oriental COCOSDA held jointly with 2013 conference on Asian spoken language research and evaluation (O-COCOSDA/CASLRE)*. IEEE, 2013, pp. 1–4.
- [22] Joachim Thiemann, Nobutaka Ito, and Emmanuel Vincent, "The diverse environments multi-channel acoustic noise database (demand): A database of multichannel environmental noise recordings," in *Proceedings of Meetings on Acoustics ICA2013*. Acoustical Society of America, 2013, p. 035081.
- [23] Yi Hu and Philippos C Loizou, "Evaluation of objective quality measures for speech enhancement," *IEEE Transactions on audio, speech, and language processing*, vol. 16, no. 1, pp. 229–238, 2007.
- [24] Cees H Taal, Richard C Hendriks, Richard Heusdens, and Jesper Jensen, "An algorithm for intelligibility prediction of time-frequency weighted noisy speech," *IEEE Transactions on Audio, Speech, and Language Processing*, vol. 19, no. 7, pp. 2125–2136, 2011.
- [25] Antony W Rix, John G Beerends, Michael P Hollier, and Andries P Hekstra, "Perceptual evaluation of speech quality (pesq)-a new method for speech quality assessment of telephone networks and codecs," in *2001 IEEE international conference on acoustics, speech, and signal processing. Proceedings (Cat. No. 01CH37221)*. IEEE, 2001, vol. 2, pp. 749–752.
- [26] ITUT Recommendation, "Vocabulary for performance and quality of service," *International Telecommunications Union—Radiocommunication (ITU-T), RITP: Geneva, Switzerland*, 2006.
- [27] Chandan KA Reddy, Vishak Gopal, and Ross Cutler, "DNS-MOS: A non-intrusive perceptual objective speech quality metric to evaluate noise suppressors," in *IEEE International Conference on Acoustics, Speech and Signal Processing (ICASSP)*. IEEE, 2021, pp. 6493–6497.